Bond-centered hydrogen in silicon studied by *in situ* deep-level transient spectroscopy

K. Bonde Nielsen, B. Bech Nielsen, J. Hansen, E. Andersen, and J. U. Andersen
Institute of Physics and Astronomy, University of Aarhus, DK-8000, Aarhus C, Denmark
(Received 24 November 1998)

In situ deep level transient spectroscopy (DLTS) has been applied to investigate *n*-type silicon implanted with protons at low temperatures. Two DLTS signals, labeled $E3'$ and $E3''$, originate from hydrogen-related donor centers. The electron emission rates of the donors are similar and the two signals are discernible only because they form and anneal differently. In *n*-type silicon, the $E3'$ and $E3''$ centers transform into negatively charged centers at $\sim$100 K and at $\lesssim$65 K, respectively. Both signals can be regenerated at 65 K: $E3'$ by forward-bias injection of holes and $E3''$ by illumination with band-gap light under reverse-bias conditions. During the $E3'$ regeneration long-range migration of hydrogen occurs, whereas $E3''$ regenerates without migration. In the space-charge layer of reverse biased diodes, $E3'$ converts into $E3''$ with an activation enthalpy of 0.44 eV in oxygen-rich material, whereas $E3''$ converts into $E3'$ with an activation enthalpy of 0.72 eV in oxygen-poor material. It is found that the density of hydrogen sites associated with $E3''$ approximately equals the oxygen concentration, whereas the density of $E3'$ sites is about $10^{23}\,\mathrm{cm}^{-3}$. These results provide further evidence for our previous assignment of $E3'$ to isolated hydrogen at a bond center site and leads to the assignment of $E3''$ to bond centered hydrogen perturbed by a nearby oxygen atom. We argue that dilated Si-Si bonds in the strain fields around impurities and defects are trapping sites for hydrogen. [S0163-1829(99)01727-0]

I. INTRODUCTION

In several steps of electronic-device processing, hydrogen is an abundant element which may influence the device performance through interaction with other impurities and imperfections. Therefore, hydrogen in silicon has been studied extensively with a number of experimental and theoretical methods,[1,2] and a fruitful interplay between experiments and theory has led to significant advances in our understanding of the structure and dynamics of this system.[3]

The structure of isolated hydrogen in crystalline silicon has been calculated by several groups.[4–8] A general consensus has emerged[3] according to which hydrogen in silicon can exist in three charge states: H^-, H^0, and H^+. The global minimum in the total energy of H^- is attained with the hydrogen atom at (or near) the interstitial tetrahedral site whereas the total-energy curves for H^0 and H^+ have global minima at the bond-center site. We denote these configurations by $H^-(T)$, H^0(BC), and H^+(BC). According to theory, hydrogen in silicon is a negative-*U* system[6,8] where either H^+(BC) or $H^-(T)$ represents the minimum in free energy for all positions of the Fermi level and H^0(BC) is always metastable. Experimental support for the negative-*U* behavior has been obtained recently.[9]

The high reactivity and room-temperature mobility of interstitial hydrogen hamper the direct observation of $H^-(T)$, H^0(BC), and H^+(BC). One way to evade this problem is to introduce hydrogen by proton implantation at cryogenic temperatures where hydrogen and (most) intrinsic defects are immobile. Then, the structures of isolated hydrogen may be studied by *in situ* applications of standard techniques.[10–13]

In *p*-type or intrinsic material, H^0(BC) converts into H^+(BC).[4–8] However, a steady-state population of H^0(BC) can be produced by illumination with band-gap light. Using this procedure, Gorelkinskii and Nevinnyi[10] observed the electron paramagnetic resonance (EPR) signal, labeled AA9, which originates from H^0(BC). The conversion of H^0(BC) into $H^-(T)$ in *n*-type silicon includes a site change as well as capture of an electron. Since the calculated energy of H^-(BC) exceeds that of H^0(BC), an enthalpy barrier may prevent the conversion from H^0(BC) to $H^-(T)$ at low temperatures. This has been confirmed experimentally: Irmscher *et al.*[11] applied deep level transient spectroscopy (DLTS) and observed a hydrogen-related donor signal $E3'$ in *n*-type silicon implanted with protons. The metastability of the $E3'$ center was established by our group and its annealing was found to match that of the AA9 signal.[12,13] On this basis, the DLTS signal $E3'$ was assigned to electron emission from H^0(BC).

This paper presents the results of a series of *in situ* DLTS measurements on *n*-type silicon implanted with protons at low temperatures. A new hydrogen-related DLTS signal $E3''$ has been identified, which is closely related to $E3'$. The electric-field dependence of the emission rates of $E3'$ and $E3''$ has been investigated, as well as the formation and annealing of both signals. The effect of hydrogen-oxygen interactions on the annealing scenario is described and it is concluded that $E3''$ originates from H^0(BC) perturbed by a nearby oxygen atom. It is suggested that quite generally H^0 will be trapped and stabilized by the strain field surrounding impurities and defects in silicon.

II. EXPERIMENTAL DETAILS

A series of diodes were prepared on *n*-type silicon substrate and low doses of protons (or deuterons) were implanted at cryogenic temperatures through the diode junction into the substrate. The defects produced and their thermal evolution were subsequently studied by *in situ* DLTS with a Semitrap DLS-82E spectrometer.[14] In the majority-carrier

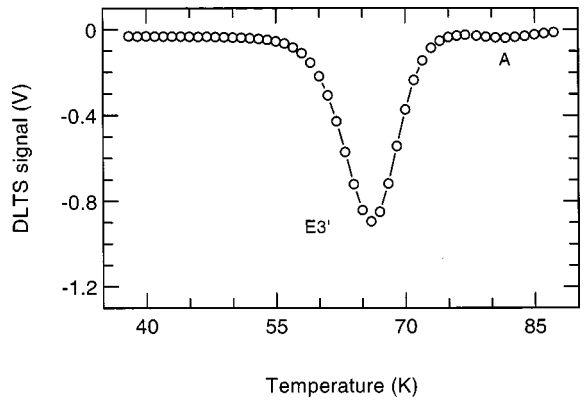

FIG. 1. DLTS temperature scan recorded with an as-implanted FZ Schottky diode. The duration of the filling pulses were 5 μs and the rate window corresponded to $e_n = 5.5\,\mathrm{s}^{-1}$.

DLTS applied in this work the thermal emission of electrons from deep centers to the conduction band was monitored as a capacitance transient $\Delta C(t)$ recorded at fixed quiescent reverse bias after the centers had been filled by a pulsed reduction of the bias (the filling pulse). The capacitance transient is connected to the temperature-dependent emission rate $e_n(T)$ by the relation $\Delta C(t) = \Delta C(0)\exp[-e_n(T)t]$ and arises as the width of the space-charge layer is gradually restored to its quiescent value during the emission. In our instrument, the filling pulse is repeated periodically with the rate ν and the ensuing capacitance transients are fed into a lock-in amplifier which, tuned to frequency ν, yields the DLTS signal through integration with a square-wave weight function. For a particular center, the temperature T_{peak} at which the DLTS signal attains its maximum value is determined by the lock-in integration according to the relation $e_n(T_{\mathrm{peak}}) = 2.17\nu$. The DLTS spectra could then be recorded either as a function of temperature with fixed ν (temperature scan) or as a function of ν at fixed temperature (frequency scan). For an electron-emitting deep center, as investigated in this work, the DLTS signal appears in the spectra as a negative peak, where the peak heigth determines the abundance of the center. Typical temperature and frequency spectra are exemplified in Figs. 1 and 2. The depth distributions of free carriers were examined by capacitance voltage (CV) profiling with a Keithley 590 capacitance analyzer. The measured free-carrier profile depends on the rate Ω_r at which the voltage is ramped and the electron emission rate e_n of the centers.[12,15,16] For high ramp rates, $\Omega_r \gg e_n$, the electrons remain attached to the centers during the measurement and the profile displays the shallow-donor profile compensated by the implantation damage. In contrast, the free-carrier profile contains a contribution from electrons emitted from the centers for slow ramp rates, $\Omega_r \ll e_n$. The difference between the slow-ramp and the fast-ramp profiles is denoted *the emission profile*. Although, it is distorted and shifted with respect to the real profile of the centers,[15,16] the integral of this profile equals the number of centers per unit area, apart from a slight renormalization.

Phosphorus-doped wafers with resistivities in the range 1–100 Ω cm of float-zone (FZ) and Czochralski-grown (CZ) silicon were used as substrates. Schottky diodes and mesa-etched p^+n diodes were produced by evaporation of a gold layer and by molecular beam epitaxial growth, respectively.

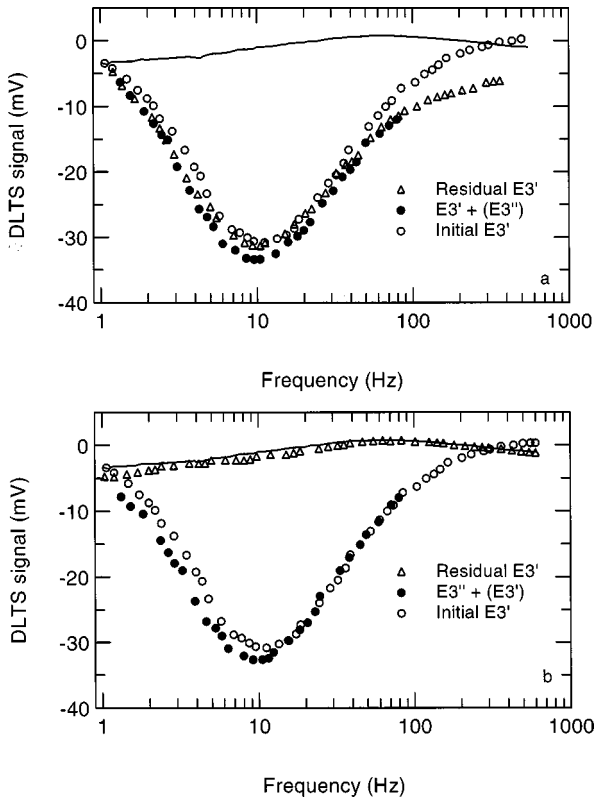

FIG. 2. (a) DLTS frequency scans recorded at 65 K with a p^+n FZ diode just after the implantation (initial $E3'$) and after zero-bias decay at 100 K (solid line). The regenerated $E3' + (E3'')$ sum signal was obtained after 20 min forward-bias injection at 80 K ($1A\,\mathrm{cm}^{-2}$) followed by 10 sec reverse-bias illumination. The residual $E3'$ signal was obtained after the diode was short-circuited at 65 K. The regenerated $E3'$ signal dominates over the regenerated $E3''$ signal. (b) $E3'' + (E3')$ sum signal obtained after zero-bias decay by 10 sec illumination under reverse bias is shown together with the residual $E3'$ obtained after subsequent short-circuiting of the diode. The signals were measured before any forward-bias injection was carried out. The regenerated $E3''$ signal dominates over the regenerated $E3'$ signal.

The junction areas were $\sim$1.3 mm^2 and an InGa alloy was rubbed onto the backside of the substrate to make Ohmic contacts. Individual diodes were cut and glued with a conducting paste onto TO-5 holders and were finally bonded with aluminum wires using ultrasonic bonding. The samples were mounted four at a time inside a vacuum chamber on a copper block in thermal contact with the cold finger of a closed-cycle He cryocooler. The four diodes were implanted individually at 40–60 K and were either short circuited or reverse biased (at 20 V) during the implantation. A 5 MV van de Graaff accelerator with a radio-frequency ion source delivered the proton or deuteron beam. The beam energy was chosen to yield an implant profile located in the middle of the depletion layer corresponding to 20 V reverse bias. For a 10-Ω cm sample, this energy is about 450 keV. The typical implantation dose was 10^9–$10^{10}\,\mathrm{cm}^{-2}$, chosen to give less than 20% compensation of the initial free-carrier density. The samples were wired for measurements on one diode at a time, with a common wire to the Ohmic backside contacts of all four diodes. In a few cases, the diodes were mounted on a TO-5 holder with a 1-mm^2 hole into which a collimating

tube was screwed. This allowed illumination of the diode from the backside through the substrate.

In most cases, the open-face front of the diodes required for implantation was exposed to the thermal radiation inside the vacuum chamber. As discussed in detail elsewhere,[17] this radiation causes a temperature-independent increase in the emissivity of both centers discussed here. To avoid this exposure, some samples were implanted through a thin gold foil, adhered to the sample holder and covering the front face of the diode.

III. RESULTS

A. Summary of previous results

Earlier,[11,12] it was shown that the DLTS signal $E3'$ is observed in p^+n CZ silicon diodes after proton implantation below ~90 K. Briefly summarized, $E3'$ has the following characteristics:[12] It originates from a hydrogen-related deep donor with an ionization enthalpy of about 0.16 eV. In an unbiased diode, $E3'$ disappears after heat treatment at ~100 K but the signal is regenerated by forward-bias injection of minority carriers at 65 K. In a reverse-biased diode, $E3'$ is stable up to ~200 K but can be recovered if the temperature has not exceeded ~250 K. The zero-bias decay at ~100 K is governed by a single atomic jump of hydrogen,[12] whereas the process controlling the reverse-bias decay is unknown. In the following, data are presented which add further information to these results.

B. Formation of hydrogen donors

A DLTS temperature scan, recorded with a Schottky diode after proton implantation into FZ silicon at 50 K, is shown in Fig. 1. The spectrum is dominated by $E3'$ but a small dip at ~80 K is associated with the oxygen-vacancy pair (*A* center).[18] In diodes with CZ substrate, the *A*-center signal is larger but $E3'$ is still dominating.

The intensity of $E3'$ accounts for a large fraction of the hydrogen implants. In a short-circuited diode the fraction is $\gtrsim$75% but it reduces to about 50% in a reverse-biased diode. The missing fraction gives rise to a new DLTS signal, denoted $E3''$, with an emission dip in the DLTS spectrum at the same temperature as for $E3'$. The initial intensity of $E3''$ corresponds to ~30% of the hydrogen implants in the reverse-biased diodes. Hence, about 80% of the implants can be accounted for by the initial $E3'$ and $E3''$ signals.

$E3'$ and $E3''$ can be distinguished on the basis of their different dynamical properties. With no bias on the diode, $E3''$ decays swiftly even at 40 K, which is the minimum temperature attainable with our setup. In 10 Ωcm *n*-type silicon, the decay proceeds at 65 K with a half time of $t_{1/2}$ ~30 ms whereas $E3'$ decays at 100 K with $t_{1/2}$~150 s under zero-bias conditions. Fortunately, reverse bias stabilizes $E3''$ and the initial intensity of the signal could be determined from a frequency scan recorded at 65 K. When we in the following refer to $E3'$ and $E3''$ as labels for two different signals it is implied that they always have been separated experimentally on the basis of their different dynamical behavior, as described above. This dynamic distinction is discussed further in the next subsection and is illustrated in Fig. 2.

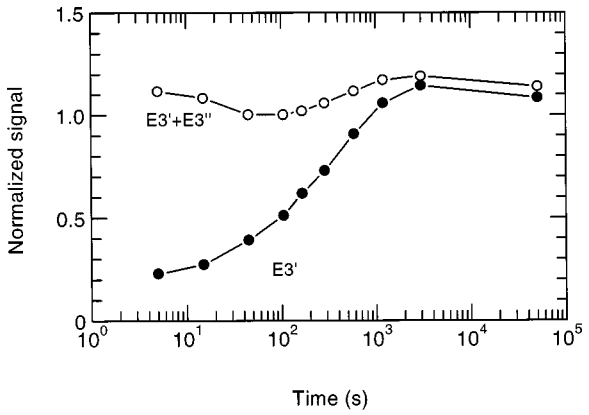

FIG. 3. Normalized intensity of $E3'$, regenerated at 65 K by forward-bias injection ($1.5A\ cm^{-2}$), shown as a function of injection time. The normalized intensity of the $E3'+E3''$ sum signal generated by illumination under reverse-bias at each time step is also shown. The signals have been normalized to the intensity of the $E3'+E3''$ signal generated just before the forward-bias injection was initiated.

$E3'$ and $E3''$ are observed after proton and deuteron implantation but neither signal is observed after implantation of helium or irradiation with 2 MeV electrons. This provides strong evidence that both $E3'$ and $E3''$ originate from hydrogen defects, as reported previously for $E3'$.

Within the uncertainty, the initial intensities of $E3'$ and $E3''$ are unaffected by the content of phosphorus in the range investigated (10^{14}–$10^{15}\,cm^{-3}$). This indicates that the $E3'$ and $E3''$ centers are not associated with phosphorus. We shall present evidence that the $E3''$ center is oxygen related in Sec. III E.

C. Regeneration of $E3'$ and $E3''$

After zero-bias decay of the initial $E3'$ and $E3''$ signals, both can be regenerated at 65 K but in different ways. $E3'$ is regenerated with high intensity by forward-bias injection of holes (~$1.5A\ cm^{-2}$ in 20 min), whereas $E3''$ is efficiently generated in a reverse-biased diode by illumination with a Nd:YAG laser from the sample backside through the 1 mm^2 hole in the TO-5 holder (1 mW on the sample for a few seconds). Typical examples of the signals generated by the two methods are shown in Fig. 2. After forward-bias injection of holes, the intensities of the signals relative to the initial $E3'$ are ~100% for $E3'$ and ~5% for $E3''$ [see Fig. 2(a)]. In contrast, the corresponding relative intensities are $\lesssim$5% for $E3'$ and ~100% for $E3''$ when the signals are regenerated by illumination of a reverse-biased diode [see Fig. 2(b)]. The intensities of $E3'$ and $E3''$ generated by either method do not change significantly when the signals are regenerated after a few additional zero-bias decays. Hence, it is possible to cycle reversibly between states of the sample in which $E3'$ or $E3''$ dominates over the other signal. This strongly suggests that $E3'$ and $E3''$ originate from two metastable defect configurations which convert to, and can be regenerated from, configurations unobserved by DLTS. Further evidence for the close relation between $E3'$ and $E3''$ is presented in Fig. 3, in which the increase of $E3'$ as a function of the duration of forward-bias injection is shown. The

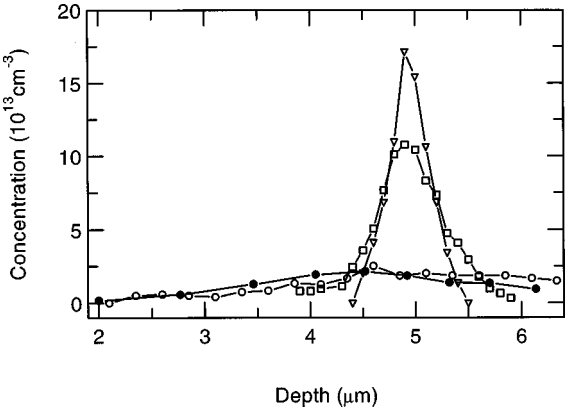

FIG. 4. Emission profiles (see text), i.e., inferred concentration profiles of the hydrogen $E3'$ center, revealing the injection induced migration of hydrogen at 65 K. The open triangles show the emission profile measured just after implantation in a p^+n FZ diode. The open squares and open circles depict the emission profile measured after one and four cycles of zero-bias decay and forward-bias injection. The solid circles show the constant-voltage $E3'$-DLTS profile measured after the fourth cycle.

concurrent decrease of $E3''$ generated on top of $E3'$ is revealed by the nearly constant intensity of the sum signal $E3'+E3''$.

There is another significant difference between the two regeneration processes. The regeneration by forward-bias injection at 65 K is accompanied by long-range diffusion of hydrogen. This is evident from Fig. 4 where the emission profile (defined in Sec. II), obtained before zero-bias decay of the initial $E3'$ signal, is shown together with the corresponding profiles measured after one and four cycles of zero-bias decay and subsequent forward-bias injection. The $E3'$ profile measured by constant-voltage DLTS (Ref. 19) after the fourth cycle is also shown for comparison. After the fourth cycle, the hydrogen is dispersed over the entire depletion region. In contrast, the recycling of $E3''$ by successive zero-bias decays and light exposures under reverse bias proceeds without resolvable redistribution of the hydrogen. Furthermore, the constant-voltage DLTS profile of $E3''$, measured after a few cycles of forward-bias injection and subsequent zero-bias decay, is identical to the $E3'$ emission profile measured prior to the last zero-bias decay. With specific reference to Fig. 4, the $E3''$ distribution measured after the fifth decay follows that of the $E3'$ distribution measured after the fourth decay. We conclude that long-range diffusion of hydrogen does not occur during illumination of reverse-biased diodes.

D. Electronic properties of $E3'$ and $E3''$

The close similarity between $E3'$ and $E3''$ is evident from Fig. 2. A detailed comparison of the two signals requires knowledge about the electric-field dependence of their emission rates. The DLTS dips of $E3'$ and $E3''$ shift towards lower temperatures (higher emission rates) when the magnitude of the electric field E increases. This indicates that $E3'$ and $E3''$ reflect electron emission from deep donor levels and that the electric-field dependence is caused by the Poole-Frenkel effect.[16]

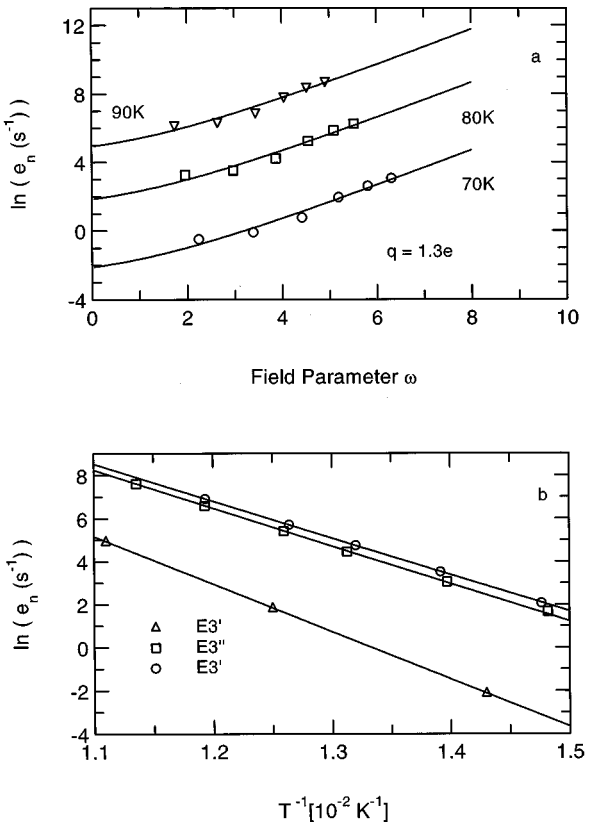

FIG. 5. (a) The emission rate e_n of $E3'$ measured at three different temperatures are plotted against the field parameter $\omega=(e^3E/\pi\varepsilon)^{1/2}/k_BT$, where E is the magnitude of the electric field, e the elementary unit of charge, T the temperature, ε the dielectric constant of silicon, and k_B Boltzmann's constant. The solid lines represent the best fit to the data obtained with the three-dimensional Hartke model (Ref. 20). The fitted parameter q is the donor charge. (b) Arrhenius plot (△) yielding the zero-field activation enthalpy $\Delta H_{\rm em}=0.175\pm0.005$ eV and preexponential factor $e_{no}=1.5\times10^8T^2$ s^{-1} of $E3'$. Included in (b) is a comparison of the $E3'$ (○) and $E3''$ (□) data obtained with $E\approx2\times10^6$ V m^{-1}.

We have examined this dependence in detail for $E3'$. In Fig. 5(a), the emission rate is plotted against the field-parameter ω proportional to $E^{1/2}$, where E is determined from CV profiles measured with high ramp rate ($\Omega_r\gg e_n$). The solid curves in the figure represent fits to the data, obtained from Hartke's three-dimensional extension[20] of the standard Poole-Frenkel analysis[16] with the donor charge q as the only adjustable parameter (common for all curves). The best fits are obtained with $q=1.3e$, but this value may vary within the limits $1\leqslant q/e\leqslant1.5$ when the uncertainty in E is taken into account. This finding supports the previous assignment of $E3'$ to a single donor.[11,12] The zero-field emission rates were obtained by extrapolation of the curves to $\omega=0$. The Arrhenius analysis of the zero-field rates of $E3'$, shown in Fig. 5(b), gives the values $\Delta H_{\rm em}=0.175\pm0.005$ eV for the ionization enthalpy and $e_0=(1.5\pm0.5)\times10^8\,T^2\,{\rm K}^{-2}\,{\rm s}^{-1}$ for the pre-exponential factor. The uncertainties quoted for $\Delta H_{\rm em}$ and e_0 include the effect of varying q within the limits stated above. In our previous work,[12] we obtained the value $\Delta H_{\rm em}=0.16\pm0.01$ eV based on the standard Poole-Frenkel analysis.[16]

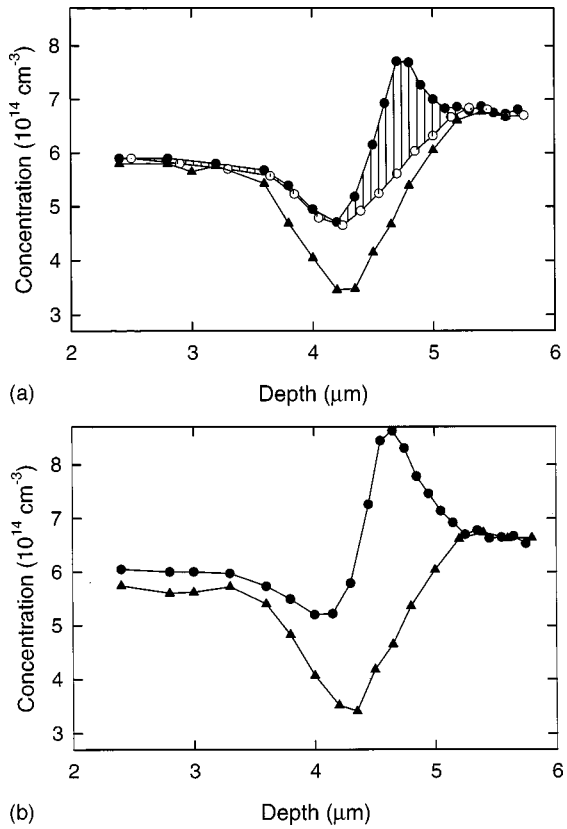

FIG. 6. (a) CV profiles recorded with fast and slow increasing voltage ramp, i.e., under conditions where $E3'$ centers are ionized (●) and nonionized (○). Also shown is the CV profile measured after zero-bias decay of $E3'$ (▲). (b) CV profiles recorded immediately after illumination with decreasing voltage ramp, i.e., under conditions where $E3''$ centers are ionized (●) and stable during profiling. The CV profile measured after zero-bias decay of $E3''$ (▲) is also shown.

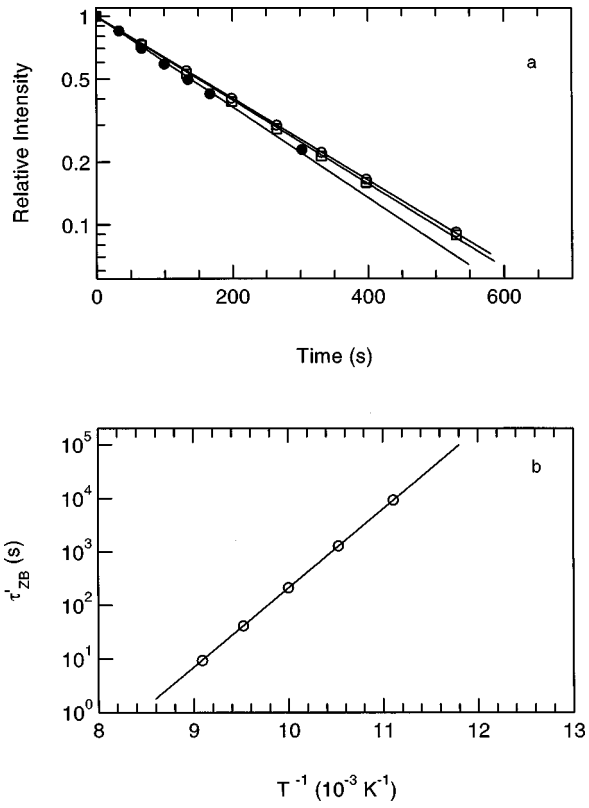

FIG. 7. (a) Relative intensity of $E3'$ as a function of zero-bias decay time at 100 K. The isothermal decay curves are shown for samples with different resistivities: 100 Ω cm FZ material (●), 10 Ω cm CZ material (○), and 1 Ω cm FZ material (□). (b) Arrhenius plot of the zero-bias decay time τ'_{ZB} in 10 Ω cm CZ material against inverse temperature. The solid line corresponds to an activation enthalpy of $\Delta H'_{ZB}=0.295\pm0.005$ eV and a pre-exponential factor $\nu'_{ZB}=(3\pm0.5)\times10^{12}$ s^{-1}.

Now we deal with the electric-field dependence of $E3''$ by direct comparison of $E3'$ and $E3''$, recorded under identical conditions in a number of different samples. The difference between the emission rates of the two signals is always minute, as exemplified by the Arrhenius plots also depicted in Fig. 5(b). The small deviation between the $E3'$ and $E3''$ data is of the same magnitude as the shift between the initial $E3'$ data and those recorded after zero-bias decay and forward-bias injection. Hence, within the limits of error, the emission properties of $E3'$ and $E3''$ are identical, which implies that also $E3''$ originates from a single donor.

The CV profiles recorded when $E3'$ dominates, at low (ionized $E3'$ donor) and at high (nonionized $E3'$ donor) ramp rates, are shown in Fig. 6(a). The number of $E3'$ centers deduced from the DLTS signal matches the hatched area between the two curves in Fig. 6(a), which implies that only a single electron is emitted per center, as expected for a single donor. Due to the instability of $E3''$ under zero bias, the CV profile could be measured only with this donor in its ionized state [see Fig. 6(b)]. The signal may in this case contain a contribution from occupied minority traps.[16] However, the close similarity between the CV profiles for ionized $E3'$ and $E3''$ centers does indicate that $E3''$ also represents emission from a single donor.

The CV profiles measured after zero-bias decay of $E3'$ and $E3''$, included in Fig. 6, are identical and display no dependence on the ramp rate (Ω_r). For $E3'$, the area between the curve measured for ionized centers prior to the decay and that measured after the decay corresponds to a drop in free charge equal to two electrons per center. Since the ionized $E3'$ center is positive (single donors), the DLTS-invisible configurations, to which the $E3'$ and $E3''$ centers convert, must be singly negatively charged.

E. Thermal decays of $E3'$ and $E3''$

1. Decays in zero-biased diodes

The zero-bias decay of $E3'$ at ~100 K involves the capture of a single electron. The decay proceeds as a first-order process, as can be seen from Fig. 7(a). The decay rate does not depend significantly on the resistivity of the sample, which shows that thermal activation rather than electron capture is the rate controlling process. Moreover, the decay curves measured for diodes on FZ and CZ substrates are identical, which suggests that oxygen does not play a role in the process. In Fig. 7(b), the Arrhenius plot obtained from isothermal annealing curves recorded at several temperatures is shown. The analysis[12] yielded the activation enthalpy $\Delta H'_{ZB}=0.293\pm0.005$ eV and the pre-exponential factor ν'_{ZB}

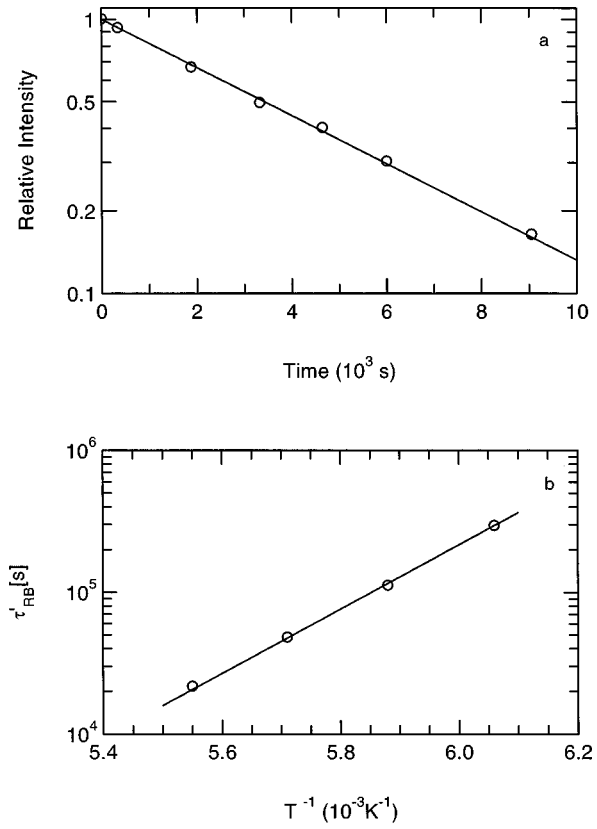

FIG. 8. (a) Relative intensity of $E3'$ as a function of reverse-bias decay time in 10 Ω cm CZ material at 175 K. (b) Arrhenius plot of the reverse-bias decay time τ'_{RB} in 10 Ω cm CZ material against inverse temperature. The solid line corresponds to an activation enthalpy of $\Delta H'_{RB}=0.44\pm0.01$ eV and a pre-exponential factor $\nu'_{RB}=(1.3\pm0.6)\times10^8\,s^{-1}$.

$=(3.0\pm0.5)\times10^{12}\,s^{-1}$. Such a pre-exponential factor is typical for a thermally activated single-jump process. Furthermore, we showed in Ref. 12 that the zero-bias decay proceeds faster in proton-implanted than in deuteron-implanted samples. This provides strong evidence that the zero-bias decay is governed by a thermally activated jump of hydrogen.

The zero-bias decay of $E3''$ is not a first-order process. The rate constant is within ~25% proportional to the free-electron density and hence electron capture seems to control this decay. It has not been possible to establish whether single jumps of hydrogen also play a role in this process.

2. Decays in reverse-biased diodes

Next, we describe the thermal decays of $E3'$ and $E3''$ in reverse-biased diodes. First we discuss the $E3'$ decay in CZ material. Also this process displays first order kinetics, as can be seen from the isothermal decay curve in Fig. 8(a). The Arrhenius plot is shown in Fig. 8(b) and from a fit to the data we find the activation enthalpy $\Delta H'_{RB}=0.44\pm0.01$ eV and the pre-exponential factor $\nu'_{RB}=(1.3\pm0.6)\times10^8\,s^{-1}$.

This value of ν'_{RB} is inconsistent with a single jump of hydrogen being the rate controlling process. We note that $\Delta H'_{RB}$ is very close to the hydrogen migration enthalpy (0.48 eV) measured at high temperatures,[21] which suggests a process controlled by hydrogen migration in a field of traps. Such a process would indeed result in a low pre-exponential factor and it would display first-order kinetics with rate constant $k_T=4\pi R_T D N_T$, where R_T is the trapping radius, D is the hydrogen diffusion constant, and N_T is the density of traps. The trap density can be estimated from the observed rate constants (e.g., $k_T\sim3\times10^{-6}\,s^{-1}$ at 165 K). With the value of D extrapolated from high-temperature data[21] ($D\sim2\times10^{-17}\,cm^2\,s^{-1}$ at 165 K) and a reasonable trapping radius, $R_T\sim2$ Å, we get $N_T\sim6\times10^{17}\,cm^{-3}$. This is substantially higher than the density of phosphorus ($5\times10^{14}\,cm^{-3}$), carbon ($\leqslant5\times10^{16}\,cm^{-3}$), hydrogen ($\leqslant2\times10^{14}\,cm^{-3}$), and implantation defects ($\leqslant4\times10^{15}\,cm^{-3}$), but it agrees roughly with the density of interstitial oxygen ($\sim10^{18}\,cm^{-3}$). The reverse-bias decay of $E3'$ in CZ material may therefore be controlled by trapping of migrating hydrogen at interstitial oxygen.

Further evidence for the role of oxygen is provided by the striking difference between the thermal decays of $E3'$ and $E3''$ in FZ and CZ material, depicted in Fig. 9. The data in part (a) of the figure were obtained from FZ material in the following way: Prior to each step in a series of isochronal heat treatments with reverse bias, $E3'$ from the previous step was removed by a zero-bias anneal at ~100 K. Then $E3''$ (predominantly) was generated by illumination and its intensity I''_0 was determined whereupon the heat treatment was carried out. Subsequently, the intensities I' of $E3'$ and I'' of $E3''$ were determined. In Fig. 9(a), I' and I'' normalized to I''_0 are plotted against the annealing temperature. The data for CZ material, shown in Fig. 9(b), were obtained in a slightly different way. After the implantation, the initial $E3'$ (and $E3''$) was removed by a zero-bias anneal at ~100 K whereupon $E3'$ (predominantly) was regenerated by forward-bias injection. Prior to each heat treatment, $E3''$ was removed by a zero-bias anneal at ~65 K and the intensity I'_0 of the residual $E3'$ was determined and used to normalize I' and I'' measured after the heat treatment. Above 220 K, the normalized $E3''$ signal was obtained in a different way. Prior to each heat treatment in this temperature range, the signal was generated by illumination and its intensity I''_0 was determined and used to normalize I'' measured after the heat treatment.

As can be seen from the figure, $E3'$ converts into $E3''$ at ~190 K in CZ material whereas the opposite conversion occurs at ~225 K in FZ silicon, where $E3'$ is stable up to ~240 K. Qualitatively, these observations confirm that the $E3'$ decay proceeds by hydrogen migration and trapping on oxygen. Because $E3'$ converts fully into $E3''$ in CZ but not in FZ material, we conclude that $E3''$ originates from an oxygen-hydrogen complex. The fact that $E3''$ is stable up to higher temperatures in CZ than in FZ material constitutes an alternative basis for this conclusion.

Since the $E3''$ sites act as traps in hydrogen diffusion, there must be an additional binding enthalpy Q associated with these sites. Observation of the conversion at ~225 K of $E3''$ into $E3'$ in FZ silicon therefore implies that the density of hydrogen sites associated with $E3'$ by far exceeds the oxygen concentration. This suggests that $E3'$ originates from hydrogen at solution sites because oxygen (together with carbon) is the most abundant defect in our FZ samples.

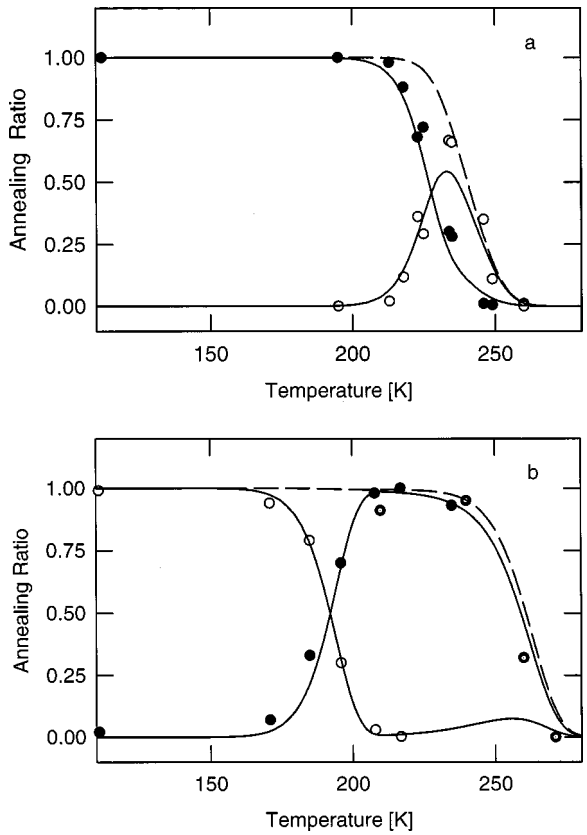

FIG. 9. (a) The normalized intensities of $E3'$ (○) and $E3''$ (●) measured in FZ material after 20-min heat treatments at different temperatures. Prior to each heat treatment, the available hydrogen was converted to $E3''$ centers. The solid lines through the data points represent the best fit to the data obtained with the diffusion model discussed in the text. The dashed lines show the normalized intensity of $E3'+E3''$ obtained from the model with the best-fit parameters. See text for further details. (b) The normalized intensities of $E3'$ (○) and $E3''$ (●) measured in CZ material after 20-min heat treatments at different temperatures. Prior to each heat treatment below 220 K, all hydrogen was removed from $E3''$ centers. Prior to heat treatments above 220 K, the available hydrogen was converted to $E3''$ centers. The solid lines through the data points represent the best fit to the data obtained with the diffusion model discussed in the text. The dashed lines show the normalized intensity of $E3'+E3''$ obtained from the model with the best-fit parameters. See text for further details.

In CZ silicon, the concentration of oxygen is higher by about two orders of magnitude and the conversion of $E3''$ to $E3'$ is shifted to $T \gtrsim 300$ K. The conversion then cannot be observed because the sum signal $E3'+E3''$ anneals at lower temperatures, $T \sim 240$ K and $T \sim 260$ K in FZ and CZ material. We ascribe these stages to hydrogen migration and trapping at sinks. This assignment is supported by the observation that neither $E3'$ nor $E3''$ can be regenerated after heat treatments above these stages.

A detailed analysis has been carried out to test our conclusions quantitatively. The analysis is based on a model in which hydrogen diffuses among solution sites ($E3'$ sites) in a field of traps ($E3''$ sites) and sinks. The details of the analysis are presented in the appendix and at this point only the major conclusions will be stated. The solid curves in Fig. 9 represent the best fit to the data obtained from the model. In the fit, the density of $E3'$ sites is set equal to the density of BC sites ($1.00\times10^{23}\,\mathrm{cm}^{-3}$) and the density of $E3''$ sites set equal to the concentration of oxygen. The best fit yields the value $Q=0.29\pm0.03$ eV for the binding enthalpy. As can be seen from the figure the agreement between fit and data points is fair. Hence, our assignments of $E3'$ to solution sites and $E3''$ to oxygen-related trap sites are quantitatively consistent with the observations. A satisfactory fit can be obtained only if $E3''$ is oxygen related and the sinks are unrelated to oxygen. The sink density needs to be $\lesssim 10^{16}\,\mathrm{cm}^{-3}$ in both FZ and CZ material in order to maintain a reasonable fit.

A few additional experimental checks of the interpretation of the reverse-bias decays were carried out. The capacitance of a reverse-biased diode was monitored as the temperature was increased at a constant rate (TSCAP measurement). No step in the capacitance-versus-temperature curve was found in a temperature range covering the reverse-bias decay stage. This strongly suggests that the process proceeds without capture or emission of free carriers, as assumed in the model.

A point of experimental concern is that the hydrogen DLTS signals might decrease due to redistribution (dispersion) of hydrogen in the space-charge layer rather than to annealing of the centers. We have carefully checked this possibility by measurements of CV and DLTS profiles. During the reverse-bias decay, the profiles broaden only slightly. We conclude that the redistribution of hydrogen does not significantly influence the measured decay curves.

IV. DISCUSSION

A. Assignment of $E3'$ and $E3''$

As mentioned in the Introduction, $E3'$ has previously been ascribed to electron emission from H^0(BC). The findings reported herein and in our previous papers[12,13] provide strong evidence for this assignment. Firstly, the $E3'$ center is hydrogen related as discussed in Sec. III B and in Ref. 12. Secondly, the observed Poole-Frenkel effect and the CV profiles in Fig. 6(a) show that the $E3'$ center is a single donor. Thirdly, from the model analysis of the reverse-bias decays, the density of hydrogen sites related to $E3'$ is $\sim 10^{23}\,\mathrm{cm}^{-3}$ which by far exceeds the density of impurities and defects. This strongly indicates that $E3'$ originates from a site associated with the perfect silicon lattice. Fourthly, the $E3'$ center is metastable (Sec. III C) and transforms into a negatively charged center (Sec. III D) as a result of zero-bias decay at $\sim$100 K. Finally, as shown in Ref. 13, the annealing behavior of $E3'$ is identical to that of the AA9 center,[10] which has been unambiguously identified with H^0(BC). This is important since it links $E3'$ to hydrogen at the BC site. On basis of all these findings we identify the nonionized $E3'$ center with H^0(BC) and thus maintain the assignment presented originally in Ref. 12.

The identical emission properties of $E3'$ and $E3''$ show that the $E3''$ center is also a single donor. $E3''$ is observed in proton-implanted but not in helium-implanted silicon, which strongly suggests that also the $E3''$ center involves hydrogen. Further evidence comes from the fact that it is possible to cycle reversibly between $E3''$ and the *hydrogen-related* $E3'$, as described in Sec. III C. Finally, the diffusion-driven conversion of $E3'$ into $E3''$ during reverse-bias decay in CZ

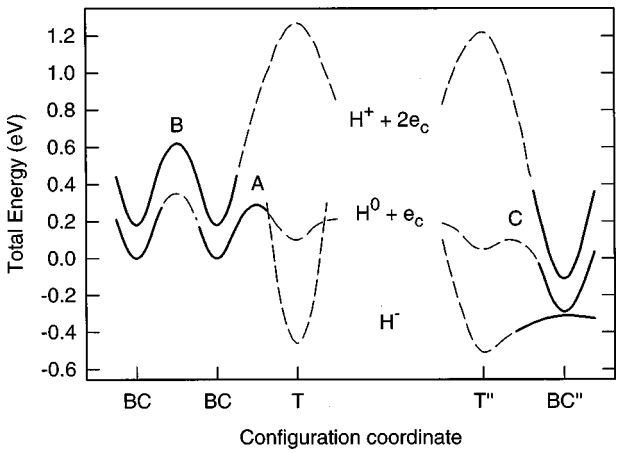

FIG. 10. Configuration diagram for the three charge states of hydrogen at isolated T and BC sites and at T'' and BC$''$ sites with a nearby interstitial oxygen atom. The zero of the energy scale has been chosen to be equal to the total energy of $H^0(BC)+e_c$. The dashed part of the curves indicates that the energies of the minima and saddle points in these regions are uncertain. The arrows indicate the thermally induced electron emissions which give rise to $E3'$ and $E3''$.

material rather unambiguously establishes the involvement of hydrogen. The differences in the reverse-bias decays in FZ and CZ silicon show that the $E3''$ center also contains an oxygen atom, as discussed in Sec. III E. The identical emission properties of $E3''$ and $E3'$ suggest that the local structures of the $E3''$ and $E3'$ centers are similar. Therefore, we tentatively identify the nonionized $E3''$ center with an H^0(BC)-O complex where bond centered hydrogen is perturbed by nearby oxygen atom(s). In view of the low concentration of hydrogen in our samples, much lower than the trap (i.e., oxygen) concentration, it is improbable that the $E3''$ center involves two or more hydrogen atoms. Also, because oxygen is immobile in silicon well below room temperature, the $E3''$ center most likely contains only a single oxygen atom.

The density of $E3''$ trap sites cannot deviate substantially from that of oxygen in our samples and remain consistent with the reverse-bias decay, as discussed in Sec. III E. Interstitial oxygen O_i, where an oxygen atom located near a BC site is bonded to the two silicon neighbors, is by far the most abundant oxygen center—even after implantation. Therefore, the $E3''$ center may more correctly be referred to as an H^0(BC)-O_i complex.

B. Configuration diagram

The sketch in Fig. 10 of the total-energy variations of the three charge states H^-, H^0, and H^+, along paths connecting neighboring BC and T sites in configuration space, complies qualitatively with the theoretical consensus.[3] We shall refer extensively to this configuration diagram in our discussion of the observed processes. A BC site associated with $E3''$, i.e., a BC site with a nearby O_i, is denoted BC$''$ and T'' labels a neighboring O_i-perturbed T site.

The zero point of the energy scale has been chosen to equal the total energy of isolated H^0 at the BC site with a free electron in the conduction band: $H^0(BC)+e_c$. The electron emission giving rise to $E3'$ is represented by the arrow from $H^0(BC)+e_c$ to $H^+(BC)+2e_c$, and the activation enthalpy, $\Delta H_{em}=0.175$ eV, for this process determines the energy of $H^+(BC)+2e_c$.

The zero-bias decay of $E3'$ involves both a change of site and electron capture (see Sec. III E) and we identify the process with $H^0(BC)+e_c \rightarrow H^-(T)$. There is no direct evidence that the hydrogen ends up at (or near) a T site and the assignment of the final configuration is guided mainly by theoretical results.[3,6,7] According to our findings, the rate of the process is controlled by the thermally activated jump of hydrogen, and the process proceeds as $H^0(BC) \rightarrow H^0(T)$ followed by $H^0(T)+e_c \rightarrow H^-(T)$. Therefore, the total energy of the saddle point in the H^0 curve, denoted A in Fig. 10, equals the activation enthalpy (0.293 eV) of the zero-bias decay. The reverse-bias decay of $E3'$ in CZ material proceeds by diffusion of ionized $E3'$ centers, i.e., H^+(BC), to traps ($E3''$ sites). The diffusion barrier is determined to be 0.44 eV, which implies that the saddle point B in Fig. 10 has the energy $0.44\,\text{eV}+0.175\,\text{eV}=0.615\,\text{eV}$.

None of the other saddle points or minima associated with isolated hydrogen in silicon can be determined on basis of this study alone. To emphasize this, the energy curves are dashed in the regions where the energies are not obtained directly. However, it is possible to make reasonable estimates of the total energies of $H^0(T)$, $H^-(T)$, and $H^+(T)$. Firstly, forward-bias injection at 45 K produces $E3'$ centers but not as efficient as injection at 65 K. As discussed below, most of the hydrogen atoms at T sites will be in the neutral charge state during forward-bias injection. Hence, the process $H^0(T) \rightarrow H^0(BC)$ may be analyzed as a simple first-order jump process with rate constant $\nu_0 \exp(-\Delta H/K_B T)$, where ΔH is approximately equal to the barrier height. If we set $\nu_0 \sim 10^{13}\,\text{s}^{-1}$, a typical value for an atomic jump process, and insert the experimental rate constant of $\sim 10^{-2}\,\text{s}^{-1}$ at $T \sim 65$ K (see Fig. 3), we obtain $\Delta H = 0.19$ eV. With this barrier, the total energy of $H^0(T)+e_c$ is 0.10 eV. Secondly, the acceptor level reported by Johnson *et al.*[9] is close to midgap. This suggests that the energy difference between $H^0(T)+e_c$ and $H^-(T)$ is about 0.56 eV, which with our estimate above would fix the energy for $H^-(T)$ to -0.46 eV. Thirdly, the ionization energy of atomic hydrogen (13.6 eV) greatly exceeds that of silicon (8.15 eV). Therefore, hydrogen is expected to be locally neutral and the configuration $H^+(T)$ then corresponds to $H^0(T)+h_\nu$, where h_ν is a valence-band hole—possibly bound to $H^0(T)$. If the binding of the hole to $H^0(T)$ is negligible, the energy difference between $H^+(T)+2e_c$ and $H^0(T)+e_c$ equals the band gap ~ 1.17 eV at 65 K. With this value, the energy of $H^+(T)+2e_c$ is ~ 1.27 eV. If the binding energy of the hole is included, the energy of $H^+(T)+2e_c$ will decrease accordingly.

Next, we discuss the energies of hydrogen trapped at O_i. From the analysis of the reverse-bias decays, the binding enthalpy of hydrogen to $E3''$ sites relative to $E3'$ sites is $Q \sim 0.29$ eV. Hence, the total energy of $H^+(BC'')+2e_c$ is obtained as the energy of $H^+(BC)+2e_c-Q \approx -0.12$ eV. Moreover, since the emission enthalpy of $E3''$ also equals 0.175 eV, the total energy of $H^0(BC'')+e_c$ will be -0.30 eV. In n-type silicon $E3''$ disappear swiftly and we assign this decay to $H^0(BC'')+e_c \rightarrow H^-(T'')$. Owing to the fact that the

rate constant of the decay scales roughly with the free-electron density, the initial step of the process is probably electron capture after which the hydrogen swiftly moves from the BC″ to the T'' site. Because the capture process proceeds efficiently at low temperatures, the energy of $H^-(BC'')$ must fall below—or be very close to—that of $H^0(BC'')+e_c$, as indicated in Fig. 10.

The variations of the energy curves in the neighborhood of the T'' site are expected qualitatively to resemble those around the isolated T site. However, there should be quantitative differences due to the nearby O_i. For the H^0+e_c curve, neither the energy minimum at T'' nor the saddle point at C (see Fig. 10) need exist. In the figure, the energy of $H^0(T'')+e_c$ has arbitrarily been chosen to be 0.05 eV and the energies of $H^+(T'')+2e_c$ and $H^-(T'')$ to be 1.17 eV above and 0.56 eV below this energy, in analogy with the estimates made for the isolated T site. As discussed in Sec. IV D, the efficient regeneration of $E3'$ under forward-bias injection suggests that the binding energy of H^0 to a T'' site relative to a T site is too small to give significant trapping during $H^0(T)$ diffusion at 65 K. On the other hand, the observed trapping at BC″ under illumination implies that the energy of $H^0(T'')$ cannot be much above that of $H^0(T)$.

C. Diffusion of hydrogen

Extrapolation of high-temperature diffusion data[21] yields a hydrogen diffusion constant of $D\sim 6\times 10^{-40}\,\mathrm{cm^2\,s^{-1}}$ at 65 K. The hydrogen profile after four 10-min forward-bias injections at 65 K (see Fig. 4) has a width of about 2 μm. This corresponds to an effective diffusion constant of $D_{\mathrm{eff}}\sim 2\times 10^{-12}\,\mathrm{cm^2\,s^{-1}}$, which is higher by 27 orders of magnitude than expected from the high-temperature data. In a recent paper Langpape *et al.*[22] reported on fast diffusion of hydrogen at low temperatures. From their fit to the observed diffusion constants[22] we find a value $\sim 7\times 10^{-18}\,\mathrm{cm^2\,s^{-1}}$ at 65 K, still five orders of magnitude below the above estimate.

The ratio between the numbers of neutral and negatively charged hydrogen atoms at T sites is equal to the ratio τ_e/τ_h between the mean times for electron capture by $H^0(T)$ and hole capture by $H^-(T)$. In the high-injection regime, the density of electrons and holes are about equal and therefore $\tau_e/\tau_h\sim\sigma_h/\sigma_e$, where σ_h and σ_e are the capture cross sections for holes and electrons. Since hole capture by a negatively charged center is very efficient compared to electron capture by a neutral center, we have $\sigma_h\gg\sigma_e$, $\sigma_h\sim 10^{-12}\,\mathrm{cm^2}$, and $\sigma_e\sim 10^{-15}\,\mathrm{cm^2}$ being typical values, and almost all the hydrogen atoms at T sites are therefore expected to be neutral during forward-bias injection.

According to theory,[3,6] the energy surface for H^0 is very flat in the open regions of the lattice, and $H^0(T)$ is expected to diffuse rapidly through the lattice even at low temperatures. This expectation is supported by the fact that normal muonium $\mu^0(T)$ in silicon, which is the analog of $H^0(T)$, is highly mobile, with a jump rate exceeding $10^{10}\,\mathrm{s^{-1}}$ at all temperatures.[23] If the value $D_{\mathrm{eff}}\sim 2\times 10^{-12}\,\mathrm{cm^2\,s^{-1}}$ is converted to a jump rate Γ, we find $\Gamma\sim 2\times 10^4\,\mathrm{s^{-1}}$ for migration of $H^0(T)$. This represents a lower limit since $H^0(T)$ eventually converts to $H^0(BC)$, which is immobile at 65 K.

D. Formation and regeneration of $E3'$ and $E3''$

1. Formation

As described in Sec. III B, the $E3'$ center $[H^0(BC)]$ is the dominating hydrogen defect produced by the proton implantation at ~40 K. Close to the end of range, the charge state of the projectile depends on the competition between electron capture and emission. Because the ionization energy of hydrogen (13.6 eV) is significantly larger than that of silicon (8.15 eV), the hydrogen atoms are most likely neutral when they become thermalized. Direct trapping of H^0 at a BC site is unlikely since a large outwards relaxation of the two silicon neighbors is required to stabilize $H^0(BC)$. Hence, we expect the hydrogen atoms to have the configuration $H^0(T)$ when they come to rest.

In a reverse-biased diode, there are essentially no free carriers and $H^0(T)$ can therefore maintain its charge state for quite some time. Also in a short-circuited diode (*n*-type material), a significant fraction of the hydrogen atoms will be in their neutral charge state *during* the implantation: By far most of the energy of the 450 keV protons is deposited in excitations of the electronic degrees of freedom over the first 5 μm of the sample. From the average energy 3.6 eV required to form an electron-hole pair[24] and a typical proton flux of $10^9\,\mathrm{cm^{-2}\,s^{-1}}$, the generation rate of electron-hole pairs is estimated to be about $3\times 10^{17}\,\mathrm{cm^{-3}\,s^{-1}}$. The lifetime τ_h of minority carries in our sample is probably within the limits $0.6\,\mu\mathrm{s}<\tau_h<10\,\mu\mathrm{s}$, where the upper limit corresponds to undamaged 10-Ω cm *n*-type material and the lower limit to silicon doped with gold atoms (potent lifetime killers) in a concentration of $10^{14}\,\mathrm{cm^{-3}}$, which well exceeds that of implantation defects. With $\tau_h=1\,\mu\mathrm{s}$, the steady state concentration of holes during the implantation is about $3\times 10^{11}\,\mathrm{cm^{-3}}$, 2–3 orders of magnitude below the density of conduction-band electrons. However, the capture cross section of holes to $H^-(T)$ probably exceeds that of electrons to $H^0(T)$ by about the same factor. Therefore, a significant part of the hydrogen atoms will be neutral during the implantation.

The expectation that a significant fraction of the hydrogen atoms at the T sites are neutral suggests that diffusion plays an important role. Application of the effective diffusion constant $D_{\mathrm{eff}}\sim 2\times 10^{-12}\,\mathrm{cm^2\,s^{-1}}$ indicates that $H^0(T)$ on average diffuses at least 500 Å during the 10-sec. implantation. This distance corresponds roughly to the average separation distance between interstitial oxygen atoms in FZ material, and hence the observation of $E3''$ directly after the implantation—even in FZ material—can be explained by diffusion.

The fact that $E3''$ is formed more efficiently in reverse-biased diodes than in short-circuited diodes is easily explained on basis of Fig. 10: $H^0(BC'')$ is unstable in *n*-type material (short-circuited diodes) because electron capture leads to a swift site change from BC″ to T''. In a reverse-biased diode, the lack of free carriers ensures that once formed $H^0(BC'')$ will be stable. In addition, when the implantation stops $H^0(T)$ will swiftly capture an electron ($\tau_{\mathrm{cap}}\sim 1\,\mu\mathrm{s}$) in the short-circuited diode whereas $H^0(T)$ survives considerably longer in the reverse-biased diode owing to the lack of carriers. Thus, the diffusion time is longer in a

reverse-biased diode whereby the trapping on BC″ sites will increase.

2. Regeneration

After zero-bias decay at ~100 K of the initial $E3'$ signal, both $E3'$ and $E3''$ can be regenerated as described in Sec. III C. According to our assignment, the zero-bias decay of $E3'$ proceeds as $H^0(BC) \rightarrow H^0(T)$ followed by electron capture $H^0(T) + e_c \rightarrow H^-(T)$. The lifetime of the intermediate configuration $H^0(T)$ is of the order 1 μs in our *n*-type material and the possibility that $H^0(T)$ diffuses to an O_i-related site before the electron capture (see Fig. 10) cannot be ruled out. However, in FZ material where the average distance to the nearest O_i is about 300 Å, this would require a jump rate between neighboring T sites of $\Gamma \sim 5 \times 10^{10}\,s^{-1}$ at 100 K. This is a very large jump rate, comparable to that reported for normal muonium,[23] and most likely the zero-bias decay of $E3'$ leads to formation of $H^-(T)$ rather than $H^-(T'')$.

$H^0(T)$ is the predominant configuration of hydrogen at T sites during forward-bias injection (see Sec. IV C). In spite of the long-range diffusion, only a minor $E3''$ signal is generated by this process. The situation is similar to that prevailing during implantation in a short-circuited diode. As soon as neutral hydrogen is trapped at $H^0(BC'')$, this structure transforms into $H^-(T'')$. Additional hole capture brings the system back to $H^0(T'')$ from which configuration the hydrogen can either jump to $H^0(BC'')$ and repeat the cycle or diffuse away to $H^0(T)$ and eventually convert to $H^0(BC)$.

The situation is quite different when the regeneration is performed by illumination under reverse bias at 65 K. Due to the low free-carrier concentration in the space-charge layer, electron and hole captures are less important. However, the laser light will induce the transition $H^-(T) + h\nu \rightarrow H^0(T) + e_c^*$, where $h\nu$ is the energy of the photon and e_c^* denotes a hot electron in the conduction band. Using a typical cross section of $10^{-15}\,cm^2$ for such a process and the photon flux of $4 \times 10^{17}\,cm^{-2}\,s^{-1}$, we estimate that essentially all $H^-(T)$ convert to $H^0(T)$ within 10 ms. As a result of the shortage of free carriers, $H^0(T)$ diffuses freely—at least for the few seconds the illumination lasts. This gives ample time[25] to become trapped as $H^0(BC'')$ which is stable because electron capture is hampered by the shortage of conduction electrons. Eventually, $H^0(BC'')$ emits an electron and becomes $H^+(BC'')$. We note from Fig. 3 that much longer times (several minutes) are needed to form $E3'$ at 65 K. This presents a simple explanation for the predominant formation of $E3''$ by illumination of reverse-biased diodes.

If the diode is short-circuited (zero-bias) below ~100 K after regeneration of $E3''$, $H^+(BC'')$ swiftly captures two electrons and converts to $H^-(T'')$ according to our configuration diagram. Subsequent illumination under reverse-bias at 65 K generates $H^0(T'')$ which for a major part transforms into $H^0(BC'')$ whereas only a minor part diffuses away and ends up primarily at other BC″ sites. Therefore, successive zero-bias decays and illumination under reverse bias proceed without resolvable redistribution of the hydrogen atoms within the depletion region.

E. General trapping mechanism

Above, the $E3''$ center was identified with a bond centered hydrogen atom, perturbed by an interstitial oxygen atom. This binding of $H^0(BC)$ to O_i can be understood in simple terms, and the underlying mechanism may be active for other impurities and defects as well.

The total energy of $H^0(BC)$ is the result of a competition between two terms of opposite sign. The first is the gain in binding energy associated with the formation of a three-centered Si-H-Si bond. This term depends critically on the Si-H-Si bond length. As the optimum Si-H-Si bond length exceeds that of the undisturbed Si-Si bond, the two silicon neighbors have to relax outwards from their perfect lattice sites to accommodate the hydrogen atom. The second term equals the increase in elastic energy owing to this relaxation. According to theory,[7] this energy is substantial: 1.8 eV for $H^0(BC)$.

In the strain field around defects or impurity atoms such as oxygen, there will be Si-Si bonds, which are longer than the 2.35 Å found in the perfect lattice. When hydrogen enters the BC site of such a dilated bond, the full gain in binding energy from the bonding is obtained but the energy cost is less than that for an unstrained Si-Si bond since less outward displacement of the two silicon neighbors is required. Therefore, the total energy of hydrogen introduced at the bond-center site of a dilated bond is lower than that of $H^0(BC)$. We suggest that any dilated bond in the strain field around impurity atoms and defects represents a trap for $H^0(BC)$. Previously, Tarnov and Street[26] and Van de Walle and Nickel[27] suggested the same trapping mechanism to apply for hydrogen in amorphous and in polycrystalline silicon.

The O_i-related structure $H^0(BC'')$ is lower in energy than $H^0(BC)$ by 0.29 eV, as discussed above. Van de Walle and Nickel[27] calculated the lowering in the formation energy ΔE_f of bond centered hydrogen as a function of the initial distortion (bond-length increase) of the Si-Si bond. They found that for distortions below ~0.3 Å, ΔE_f equals 0.46 eV per 0.1 Å initial distortion. With this number, the initial distortion of the Si-Si bond required to yield 0.29 eV binding is only 0.06 Å. According to theoretical calculations,[28] the distance between two silicon atoms directly bonded to an interstitial oxygen atom is 0.84 Å larger than the 2.35 Å of an unstrained Si-Si bond. With such a large value, it seems realistic that Si-Si bonds dilated by ~0.06 Å may exist somewhere in the proximity of O_i.

F. Comparison with previous work

Based on studies of muonium μ^0 in silicon, a configuration diagram of this light ''hydrogen isotope'' was presented recently.[29,30] Qualitatively, the diagram resembles the left-hand side of Fig. 10. In Table I, the activation enthalpies derived from the muon work are compared with those reported here. As can be seen from the table, there is close agreement between the ionization enthalpies of the $H^0(BC)$ and $\mu^0(BC)$ donors. Likewise, the activation enthalpies of the equivalent processes $H^0(BC) + e_c \rightarrow H^-(T)$ and $\mu^0(BC) + e_c \rightarrow \mu^-(T)$ are very similar. The enthalpy for $\mu^0(T) \rightarrow \mu^0(BC)$ was found to be 0.38 eV in Ref. 30 which is somewhat larger than the crude estimate 0.2 eV found for the similar process in Sec. IV B. We note that within a single-jump model, an activation enthalpy of 0.38 eV is too large to comply with the observed regeneration rate of $E3'$ at 65 K. Finally, we find that the migration process

TABLE I. Comparison of the activation enthalpies ΔH associated with isolated hydrogen and muonium in silicon.

Hydrogen[a]		Muonium[b]	
Assigned process	ΔH (eV)	Assigned process	ΔH (eV)
$H^0(BC) \rightarrow H^+(BC) + e_c$	0.175	$\mu^0(BC) \rightarrow \mu^+(BC) + e_c$	0.21
$H^0(BC) + e_c \rightarrow H^-(T)$	0.293	$\mu^0(BC) + e_c \rightarrow \mu^-(T)$	0.31
$H^0(T) \rightarrow H^0(BC)$	~0.2	$\mu^0(T) \rightarrow \mu^0(BC)$	0.38
$H^+(BC) \rightarrow H^+(BC)$	0.44	$\mu^+(BC) \rightarrow \mu^+(BC)$	
$H^+(BC) + e_c \rightarrow H^0(T)$		$\mu^+(BC) + e_c + \mu^0(T)$	0.40
$H^-(T) \rightarrow H^0(T) + e_c$		$\mu^-(T) \rightarrow \mu^0(T) + e_c$	0.56

[a]Data obtained in this work.

[b]Data from Refs. 29 and 30.

$H^+(BC) \rightarrow H^+(BC)$ has an activation enthalpy of 0.44 eV, close to the 0.40 eV ascribed to the process $\mu^+(BC) + e_c \rightarrow \mu^0(T)$ in Refs. 29 and 30. This suggests that the jump of μ^+ out of the BC site may be the rate controlling process also in the muonium work.

In a previous study,[31] we have identified local vibrational modes of two oxygen-hydrogen complexes labeled OH_I and OH_{II}. Based on the frequencies of the observed hydrogen and oxygen modes together with the results of *ab initio* calculations, OH_I and OH_{II} were identified with complexes in which $H^+(BC)$ is stabilized by a nearby O_i. The modes of OH_{II} anneal out at ~230 K which is in close agreement with the annealing temperature expected for $E3''$ in these samples. Hence, the $E3''$ and OH_{II} centers may be identical. Further work is needed to clarify this possibility.

Finally, we should like to comment on the carbon-hydrogen donor CH^0, which was originally observed by Endrös.[32] This donor has an ionization enthalpy of about 0.16 eV and it is stable at 315 K under reverse-bias conditions but anneals within ~1 min at this temperature under zero bias.[32,33] Thus, the properties of CH^0 are qualitatively similar to those of the $E3'$ and $E3''$ centers but CH^0 is stable to much higher temperatures, and neither $E3'$ nor $E3''$ is identical to the CH^0 signal. Endrös,[32] Csaszar and Endrös,[33] and Kamiura *et al.*[34] identified the CH^0 defect with a hydrogen atom residing at the BC site between a substitutional carbon atom C_s and a substitutional silicon atom. Recently, Kamiura *et al.*[35] provided strong evidence for this structure by uniaxial stress measurements. At a first glance, it might be expected that the donor level of CH^0 would be very different from that of $H^0(BC)$ but density functional calculations[36] revealed that this expectation may be incorrect.

The close proximity of the hydrogen and carbon atoms implies that direct bonding plays an important role. Thus, the higher thermal ''stability'' of CH^0 is hardly surprising. Although CH^0 may be described as an C_s-H(BC) complex and qualitatively has the same properties as O_i-H(BC) (the $E3''$ center), this structure cannot be discussed in a meaningful way on basis of the general trapping mechanism presented above.

V. SUMMARY

Low-temperature proton implantation into crystalline silicon produces two DLTS signals $E3'$ and $E3''$, which represent electron emission from deep donors. Both donors are hydrogen-related and within limits of error, they have identical emission properties with an activation enthalpy of 0.175 eV. Both signals can be regenerated after zero-bias decay, which sets in at ~100 K for $E3'$ and below 40 K for $E3''$.

Based on the thermally induced decays of $E3'$ and $E3''$ in FZ and CZ material under zero-bias and reverse-bias conditions together with our previous findings, the $E3'$ center is identified with $H^0(BC)$ and the $E3''$ center with $H^0(BC)$ stabilized by a nearby O_i. The binding enthalpy of $H^0(BC)$ to O_i is found to be 0.29 eV.

A configuration diagram has been constructed and used to explain the formation and regeneration properties of both signals. The configuration diagram is largely consistent with that suggested from muonium studies.

We find that hydrogen can diffuse rapidly in silicon at low temperatures. According to our assignment, $H^0(T)$ is the migrating agent and at 65 K the effective diffusion constant exceeds the value extrapolated from high-temperature data by 27 orders of magnitude.

A general trapping mechanism for H(BC) is suggested. It is argued that the dilated Si-Si bonds in the strain field around defects and impurity atoms act as trapping sites for H(BC). We estimate that the initial elongation of the Si-Si bond required to account for the observed binding energy 0.29 eV is about 0.06 Å.

ACKNOWLEDGMENTS

This work has been supported by the Danish National Research Foundation through the Aarhus Center for Advanced Physics (ACAP). Pia Bomholt is gratefully acknowledged for preparing the diodes applied in this work.

APPENDIX

The starting point for the analysis is the set of rate equations

$$\frac{dh'}{dt} + \frac{dh''}{dt} + \frac{dh^s}{dt} = 0, \tag{A1}$$

$$\frac{dh''}{dt} = k''h' - g''h'', \tag{A2}$$

$$\frac{dh^s}{dt} = k^s h, \tag{A3}$$

where h', h'', and h^s are the fractions of hydrogen atoms present as $E3'$ centers, $E3''$ centers, and bound to sinks. The first equation follows from conservation of the number of hydrogen atoms in the depletion layer. The term $k''h'$ gives the rate of diffusion and trapping of hydrogen at oxygen ($E3''$ traps) and $g''h''$ gives the corresponding detrapping rate. The last equation accounts for the diffusion and trapping of hydrogen atoms at sinks. The effect of hydrogen saturation of $E3''$ trapping sites has been disregarded in the second equation. This assumption is well fulfilled, because the concentration of oxygen by far exceeds that of hydrogen in our samples.

A general solution to Eqs. (A1)–(A3) is easily derived. We are interested only in the two solutions defined by the initial conditions that at time $t=0$ all hydrogen atoms either occupy solution ($E3'$) sites or trap ($E3''$) sites, i.e., the two cases where $h'=1 \wedge h''=0$ or $h'=0 \wedge h''=1$ at time $t=0$. If the constants Γ and γ are defined by

$$\Gamma \equiv \frac{1}{2}(k''+g''+k^s), \tag{A4}$$

$$\gamma \equiv \sqrt{\Gamma^2 - k^s g''} \tag{A5}$$

the two solutions corresponding to a heat treatment with duration time t are given by the following.

First case: $h'=1 \wedge h''=0$ *at time* $t=0$:

$$h' = \frac{1}{2\gamma}[(\gamma-\Gamma+g'')e^{-(\Gamma-\gamma)t} + (\gamma+\Gamma-g'')e^{-(\Gamma+\gamma)t}], \tag{A6}$$

$$h'' = \frac{k''}{2\gamma}[e^{-(\Gamma-\gamma)t} - e^{-(\Gamma+\gamma)t}]. \tag{A7}$$

Second case: $h'=0 \wedge h''=1$ *at time* $t=0$:

$$h' = \frac{g''}{2\gamma}[e^{-(\Gamma-\gamma)t} - e^{-(\Gamma+\gamma)t}], \tag{A8}$$

$$h'' = \frac{1}{2\gamma}[(\gamma+\Gamma-g'')e^{-(\Gamma-\gamma)t} + (\gamma-\Gamma+g'')e^{-(\Gamma+\gamma)t}]. \tag{A9}$$

Since we are dealing with diffusion in a field of traps and sinks, the rate constants k'', g'', and k^s may be expressed by the equations

$$k'' = 4\pi R'' D N'', \tag{A10}$$

$$g'' = 4\pi R'' D N' e^{-Q/K_B T}, \tag{A11}$$

$$k^s = 4\pi R^s D N^s, \tag{A12}$$

where N', N'', and N^s are the density of solution ($E3'$) sites, traps ($E3''$ centers), and sinks. R'' and R^s are the trapping radii associated with $E3''$ and sink sites, and Q is the binding enthalpy of hydrogen to an $E3''$ site relative to a solution site.

Since the conversion from $E3'$ into $E3''$ at ~190 K in CZ silicon is total, k'' exceeds by far g'' in this temperature range. According to Eqs. (A4)–(A6) this implies that in this case h' may to a good approximation be expressed as

$$h' \approx e^{-(k''_{CZ}+k^s_{CZ})t}, \tag{A13}$$

where the subscript CZ refers to the material. Hence, the $E3'$ decay in CZ silicon should proceed as a first order process in accordance with our observations. With the parameters obtained from the Arrhenius analysis, $\Delta H'_{RB} = 0.44 \pm 0.01$ eV and $\nu'_{RB} = (1.3 \pm 0.6) \times 10^8\ s^{-1}$, $k''_{CZ} + k^s_{CZ}$ can be calculated from

$$k''_{CZ} + k^s_{CZ} = \nu'_{RB} e^{-\Delta H'_{RB}/K_B T}. \tag{A14}$$

Using this expression and Eqs. (A10)–(A12) we now get

$$k'' = \frac{N''}{N''_{CZ}}\left(1 + \frac{R^s N^s_{CZ}}{R'' N''_{CZ}}\right)^{-1} \nu'_{RB} e^{-\Delta H'_{RB}/K_B T}, \tag{A15}$$

$$k^s = \frac{N^s}{N^s_{CZ}}\left(1 + \frac{R'' N''_{CZ}}{R^s N^s_{CZ}}\right)^{-1} \nu'_{RB} e^{-\Delta H'_{RB}/K_B T}, \tag{A16}$$

$$g'' = \frac{N'}{N''} k'' e^{-Q/K_B T}. \tag{A17}$$

The subscript CZ again refers to the values attained in CZ material. From Eqs. (A6)–(A9) and (A15)–(A17), the ratio of the numbers of hydrogen atoms occupying $E3'$ and $E3''$ sites can be calculated as a function of temperature for a specific choice of the parameters t, N'/N'', N^s/N^S_{CZ}, N''/N''_{CZ}, N^s_{CZ}/N''_{CZ}, R^s/R'', and Q. The solid curves in Fig. 9 represent the best fit to the data points obtained in the following way: t was fixed at the annealing time (20 min) at each step. The density of $E3'$ sites was set equal to that of bond center sites: $N' = 1.00 \times 10^{23}\ cm^{-3}$ in both FZ and CZ material. The density of $E3''$ sites was set equal to the approximate concentration of interstitial oxygen: $N'' = 10^{16}\ cm^{-3}$ in FZ and $N'' = 10^{18}\ cm^{-3}$ in CZ material. The density of sink sites was $N^s = 7.5 \times 10^{15}\ cm^{-3}$ in both FZ and CZ material. Finally, we set $R^s/R''=1$, corresponding to equal trapping radii for the $E3''$ traps and the sinks. With these choices of parameters, the only free parameter used in our fit was the binding enthalpy Q.

A reasonable fit to all the data cannot be obtained if any of the densities N', N'', and N^s are changed by more than a factor of 4 relative to the numbers stated above. Furthermore, within reasonable limits ($0.2 \leqslant R^s/R'' \leqslant 5$), the best-fit value of Q does not depend strongly on the ratio R^s/R''. We estimate that the resulting uncertainty on Q is about 0.03 eV.

[1] See *Hydrogen in Semiconductors*, edited by J. I. Pancove and N. M. Johnson, Semiconductors and Semimetals Vol. 34 (Academic, Boston, 1991), and references therein.
[2] See S. J. Pearton, J. W. Corbett, and M. Stavola, *Hydrogen in Crystalline Semiconductors* (Springer-Verlag, Berlin, 1992), and references therein.
[3] S. K. Estreicher, Mater. Sci. Eng., R. **14**, 314 (1995).
[4] S. K. Estreicher, Phys. Rev. B **36**, 9122 (1987).
[5] P. Deák, L. C. Snyder, and J. W. Corbett, Phys. Rev. B **37**, 6887 (1988).
[6] C. G. Van de Walle, P. J. H. Denteneer, Y. Bar Yam, and S. T. Pantelides, Phys. Rev. B **39**, 10 791 (1989).
[7] R. Jones, Physica B **170**, 181 (1991).
[8] K. J. Chang and D. J. Chadi, Phys. Rev. Lett. **62**, 937 (1989).
[9] N. M. Johnson, C. Herring, and C. G. Van de Walle, Phys. Rev. Lett. **73**, 130 (1994).
[10] Yu. V. Gorelkinskii and N. N. Nevinnyi, Pis'ma Zh. Tekh. Fiz. **13**, 105 (1987) [Sov. Tech. Phys. Lett. **13**, 45 (1987)]; Physica B **170**, 155 (1991).
[11] K. Irmscher, H. Klose, and K. Maass, J. Phys. C **17**, 6317 (1984).
[12] B. Holm, K. Bonde Nielsen, and B. Bech Nielsen, Phys. Rev. Lett. **66**, 2360 (1991).
[13] B. Bech Nielsen, K. Bonde Nielsen, and J. R. Byberg, in *Defects in Semiconductors 17*, edited by H. Heinrich and W. Jantsch, Materials Science Forum Vols. 143–147 (Trans-Tech, Aedermannsdorf, Switzerland, 1994), p. 909.
[14] G. Ferenczi, J. Boda, and T. Pavelka, Phys. Status Solidi A **94**, K119 (1986).
[15] L. C. Kimerling, J. Appl. Phys. **45**, 1839 (1974).
[16] P. Blood and J. W. Orton, *The Electrical Characterization of Semiconductors: Majority Carriers and Electron States* (Academic, London, 1992).
[17] K. Bonde Nielsen and E. Andersen, J. Appl. Phys. **79**, 9385 (1996).
[18] L. C. Kimmerling, in *Radiation Effects in Semiconductors 1976*, Conference Series No. 31, edited by N. B. Urli and J. W. Corbett (The Institute of Physics, Bristol, 1977), p. 221.
[19] See *The Electrical Characterization of Semiconductors: Majority Carriers and Electron States*, (Ref. 16), Chap. 12.
[20] J. L. Hartke, J. Appl. Phys. **39**, 4871 (1968).
[21] A. Van Wieringen and N. Warmoltz, Physica (Amsterdam) **22**, 849 (1956).
[22] Ch. Langpape, S. Fabian, Ch. Klatt, and S. Kalbitzer, Appl. Phys. A: Solids Surf. **64**, 207 (1997).
[23] B. D. Patterson, Rev. Mod. Phys. **60**, 69 (1988).
[24] K. G. McKay and K. B. McAfee, Phys. Rev. **91**, 1079 (1953).
[25] An upper limit on the typical time for $H^0(T)$ to become trapped at $H^0(BC'')$ may be estimated from the effective diffusion constant $D_{\rm eff} \sim 2\times10^{-12}\,{\rm cm^2\,s^{-1}}$ and a reasonable trapping radius of about 5 Å. From this we get that the trapping time in FZ material is less than 1 min.
[26] E. Tarnow and R. A. Street, Phys. Rev. B **45**, 3366 (1992).
[27] C. G. Van de Walle and N. H. Nickel, Phys. Rev. B **51**, 2636 (1995).
[28] R. Jones, A. Umerski, and S. Öberg, Phys. Rev. B **45**, 11 321 (1992).
[29] R. L. Lichti (private communication).
[30] B. Hitti, S. R. Kreitzman, T. L. Estle, E. S. Bates, M. R. Dawdy, T. L. Head, and R. L. Lichti, Phys. Rev. B **59**, 4918 (1999).
[31] B. Bech Nielsen, K. Tanderup, M. Budde, K. Bonde Nielsen, J. L. Lindström, R. Jones, S. Öberg, B. Hourahine, and P. Briddon, in *Defects in Semiconductors 19*, edited by G. Davies and H. Nazaré, Materials Science Forum Vols. 258–263 (Trans-Tech, Uetikon-Zuerich, Switzerland, 1997), p. 391.
[32] A. L. Endrös, Phys. Rev. Lett. **63**, 70 (1989).
[33] W. Csaszar and A. L. Endrös, Mater. Sci. Eng., B **36**, 112 (1996).
[34] Y. Kamiura, M. Yoneta, Y. Nishiyama, and F. Hashimoto, J. Appl. Phys. **72**, 3394 (1992).
[35] Y. Kamiura, N. Ishiga, and Y. Yamashita, Jpn. J. Appl. Phys., Part 2 **36**, L1419 (1997).
[36] P. J. Denteneer, C. G. Van de Walle, and S. T. Pantelides, Phys. Rev. Lett. **62**, 1884 (1989).